

Electronic Structure and Electrochemical Properties of Garnet Type $\text{Li}_7\text{La}_3\text{Zr}_2\text{O}_{12}$ Solid Electrolytes Doped with Ta and Nb

Guo Yifeng¹, Xinghua Liang^{2,*}, Li Xinqi^{2,*}, Xingtao Jiang²

¹ School of Mechanical Engineering, ChengDu University, ChengDu,. 610106, China.

² Guangxi Key Laboratory of Automobile Components and Vehicle Technology, Guangxi University of Science & technology, Liuzhou 545006, China;

*E-mail: lxh304@aliyun.com

Received: 8 November 2021 / Accepted: 8 December 2021 / Published: 2 February 2022

The migration of lithium ions in the solid electrolyte is the main limiting factor that determines the rate and cycle performance of lithium-ion batteries. Based on the first-principles method of DFT, the electronic structure of $\text{Li}_7\text{La}_3\text{Zr}_2\text{O}_{12}$ doped with Ta and Nb is studied, and the structure optimization, energy band, density of states and population analysis are carried out. The calculation results show that the lowest total energy of Ta doping system is 47307.28eV, and the structure is more stable. Due to the effect of different orbit electrons of Ta、Nb, the energy required for electron or hole transition is reduced, and the conductivity is improved, and the Ta doping is low to 2.74eV, which is more advantageous to improve the conductivity. The population analysis shows that the Ta-O bond length of the $\text{Li}_7\text{La}_3\text{Zr}_{1.75}\text{Ta}_{0.25}\text{O}_{12}$ system is 2.1717Å, and the stability is better. The Li-Li bond length of the Ta doping system is the shortest, which is beneficial to increase the Li vacancy concentration and thus improve the electrical conductivity.

Keywords: $\text{Li}_7\text{La}_3\text{Zr}_2\text{O}_{12}$; First principle; Electronic structure; Ionic conductivity

1. INTRODUCTION

Energy and environment are two major problems facing the world today. As a secondary energy source, electric energy can not only solve energy and environmental problems, but also realize energy storage and conversion. As the main carrier of electric energy, battery has been widely used in transportation, communication equipment, energy storage, electric tools and other major fields [1,3]. Traditional lithium-ion batteries use liquid electrolyte, which is easy to generate holes and dendrites in the charging and discharging process. When the temperature is too high, it is easy to cause fire and even explosion [4]. All-solid-state lithium ion battery adopts non-flammable and non-volatile solid electrolyte to replace electrolyte, which can fundamentally solve the safety problem of liquid batteries [5].

Solid electrolyte, as a key material of all-solid lithium battery, lithium-sulfur battery and new lithium-air battery, has attracted extensive attention of researchers [6,8]. Among them, garnet solid electrolyte is regarded as one of the most promising solid electrolytes because of its advantages of good electrochemical stability, wide electrochemical window and high conductivity [9]. $\text{Li}_7\text{La}_3\text{Zr}_2\text{O}_{12}$ (LLZO) has tetragonal phase and cubic phase structure. The tetragonal phase structure has good thermal stability, but the ionic conductivity is lower than that of cubic phase [10,11]. Studies have shown that the conductivity of cubic ions can reach 10^{-4}S/cm [12]. Stability and conductivity are the key factors influencing the material performance and electrochemistry performance of the battery. The tetragonal phase structure is more stable than the cubic phase structure at room temperature. The all solid state battery assembled with tetragonal LLZO has better stability in the charge and discharge process, which is conducive to improving the battery life. Therefore, improving its conductivity through certain means is the key problem to be solved by tetragonal LLZO.

First-principles calculation is a commonly used method to study the microstructure and properties of matter. Bernstein et al [13] and Adams et al [14] based on first principles, concluded that Li^+ in $\text{Li}_7\text{La}_3\text{Zr}_2\text{O}_{12}$ structure is orderly distributed in tetragonal phase, and increasing the concentration of lithium vacancy can reduce the temperature of phase transition. Experiments show that the phase transition temperature is the lowest when the lithium content is about 6.5 [15]. Adams et al [14] think the transition of Li^+ between octahedrons would be hindered by the occupation of tetrahedrons, and the tetrahedron vacancy could be increased through high-price doping to improve the conductivity. Miara et al [16] through calculation shows that different elements doping can change lattice parameters, which affect the conductivity, and is associated with Li^+ space and the concentration. The experiment also proves doping of elements can change Li^+ vacancy concentration and improve conductivity. In addition, a large number of studies have shown that the concentration of Li vacancy or Li can be increased by heterovalent cation doping, and its stability and ionic conductivity can be improved. Such as Li doped Al^{3+} , La doped Zn^{2+} , Zr doped Ta^{5+} , Nb^{5+} can improve the ionic conductivity of LLZO [17].

On the basis of this research, based on the first principle, this paper calculates the structure of LLZO, Ta^{5+} and Nb^{5+} doped LLZO model, analyzes and compares the changes of electronic structure such as energy band structure, atomic layout and density of states of the three models, discusses the influence of element doping on the electronic structure and properties of $\text{Li}_7\text{La}_3\text{Zr}_2\text{O}_{12}$.

2. MODEL CONSTRUCTION AND CALCULATION METHODS

2.1 Model construction

The structure space group of $\text{Li}_7\text{La}_3\text{Zr}_2\text{O}_{12}$ tetragonal phase [9,18] is $I4_1/acd$, the occupying rate is $a=13.134(4)\text{\AA}$, $c=12.663(8)\text{\AA}$, $c/a=0.9641$, $\alpha=\beta=\gamma=90^\circ$. The crystal structure framework is composed of hexahedron LaO_8 and octahedron ZrO_6 . Li^+ occupies three positions of 8a of tetrahedron and 16f、32g of octahedron position. The occupation rate at the octahedral position is 1, but it is empty at the 16e position of tetrahedron [19, 21]. The lithium ions are orderly arranged in LLZO. There are few short-range interactions and clusters between lithium ions, and the ionic conductivity is low. According to the

basic spatial structure and lattice parameters of LLZO, the tetragonal LLZO supercell is obtained in combination with ICSD database. Due to the large number of atoms, in order to improve the calculation efficiency, the protocell structure is obtained according to the principle of symmetry, as shown in Figure 1-1.

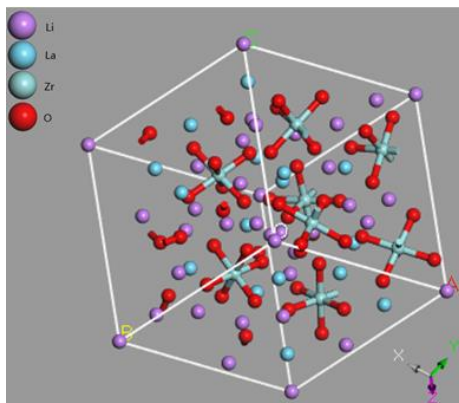


Figure 1-1 Schematic diagram of $\text{Li}_7\text{La}_3\text{Zr}_2\text{O}_{12}$ cell structure

LLZO crystal structure contains a large number of elements and each atom occupies a different position in the spatial structure, which has a certain influence on the determination of doping position and calculation and analysis. Therefore, before determining the doping position, the doping calculation was carried out for different atom positions of different elements. Through a large number of calculations, it was shown that the total energy difference obtained by doping at different positions was within 0.2eV, and within the allowable error range. In order to reduce the amount of calculation, the influence of atomic position on the total energy was ignored.

2.2 Calculation methods

In this paper, the CASTEP module of MS software is used to complete the structural optimization, energy band and state density of different models based on density functional theory. In the calculation, PBE functional method of generalized gradient approximation (GGA) was used to correct the exchange correlation potential of electron-electron interaction, and ultra-soft pseudopotential plane method (UPPW) was used to calculate the interaction potential between ions and valence electrons for all elements. The valence electrons selected for atomic pseudopotential calculation were: Li $1s^2 2s^1$, O $2s^2 2p^4$, Zr $4s^2 4p^6 4d^2 5s^2$, La $5s^2 5p^6 5d^1 6s^2$, Ta $5d^3 6s^2$, Nd $4f^4 5s^2 5p^6 6s^2$.

The relevant parameters of structural optimization were set as follows: the calculation accuracy was fine, the truncation kinetic energy of plane wave basis group was 340eV, the step length was 150, the calculation of Brillouin region was carried out by Monkhorst-Packk point grid of $4 \times 4 \times 4$, and the convergence standard was as follows: Total energy poor convergence threshold $dE/ion=1.0 \times 10^{-5}$ eV, forces of convergence threshold $|F|_{max}=0.3$ eV/Å, the displacement convergence threshold $|dR|_{max}=1.0 \times 10^{-3}$ Å, convergence threshold stress component $|S|_{max}=5.0 \times 10^{-2}$ GPa. When calculating energy

band and state density, relevant parameter values should be adjusted according to the model structure size and optimization parameter settings to ensure convergence. Set the calculation accuracy to fine, and set the truncation kinetic energy to 500eV, which should be greater than the value set for structural optimization. The self-consistent process adopts $5 \times 5 \times 5$ K-point grid iteration, and the convergence accuracy is 2.0×10^{-6} eV.

3. CALCULATION RESULTS AND ANALYSIS

3.1 Atomic structure

Ta、Nb element has high valence state, which improves stability and ionic conductivity of LLZO [22]. Structural symmetry was cancelled before element replacement, and Ta、Nb element was selected to replace Zr atoms(0.375,0.125,0,75) respectively to obtain models of $\text{Li}_7\text{La}_3\text{Zr}_{1.75}\text{Ta}_{0.25}\text{O}_{12}$ and $\text{Li}_7\text{La}_3\text{Zr}_{1.75}\text{Nb}_{0.25}\text{O}_{12}$, as shown in Figure 3-1.

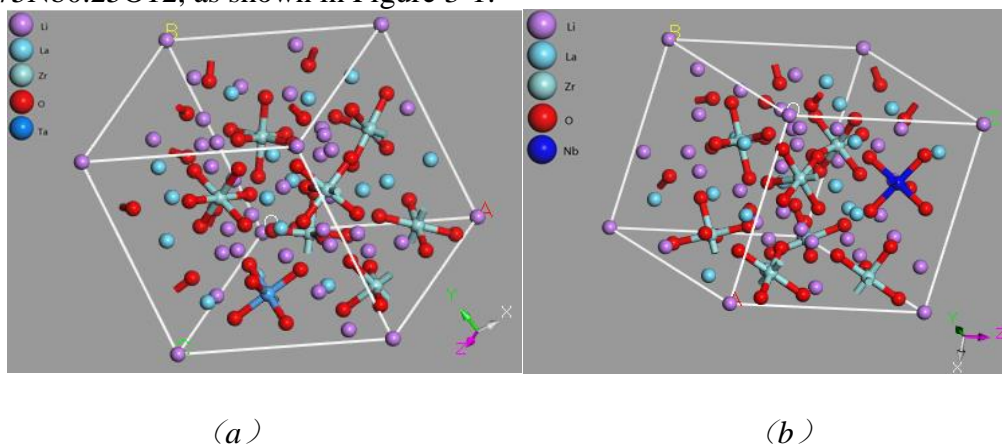


Figure 3-1 $\text{Li}_7\text{La}_3\text{Zr}_{1.75}\text{Ta}_{0.25}\text{O}_{12}$ (a) and $\text{Li}_7\text{La}_3\text{Zr}_{1.75}\text{Nb}_{0.25}\text{O}_{12}$ (b) models

3.2 Structural optimization and total energy

The three models were optimized according to the minimum total energy principle, and the total energy and lattice parameters were obtained, as shown in Table 3-1. It can be seen from the table that compared with the initial LLZO value ($a=13.134(4)\text{\AA}$, $c=12.663(8)\text{\AA}$), after the optimization of the LLZO structure, the protocell volume $V=1138.34\text{\AA}^3$ and the lattice constant increased, but the error was only 1.68%, which indicates that the model is correct and reliable within the allowable range of pseudopotential plane wave method. The doping of high valence cations at Zr site leads to the change of symmetry and crystal structure. The lattice size of the Ta doped protocell model increases, and the total energy decreases to -47307.28eV , enhancing the structural stability. The substitution of element Nb leads to a slight decrease in lattice parameters, a decrease in protocell volume, and an increase in total energy, indicating that the stability of the system decreases.

The decrease of the system energy indicates that the stability of the crystal structure is improved. The structure of the material is not easy to be destroyed in the process of lithium ion embedment and release, showing high cycle stability and life [23,24]. Doping of different elements leads to different changes in crystal structure, especially doping of high-valence cations cations, which changes the size of La-O dodecahedron and Zr-O octahedron, thus affecting the stability of crystal structure and ionic conductivity [22,25,26].

Table 3-1. The lattice constants and total energy of the unit cell model after optimization of doping with different elements

Model	a(Å)	b(Å)	c(Å)	A(°)	B(°)	Γ(°)	Total Energy(eV)
Li ₇ La ₃ Zr ₂ O ₁₂	11.3979	11.3979	11.3918	108	108	111	-47039.74
Li ₇ La ₃ Zr _{1.75} Ta _{0.25} O ₁₂	11.4131	11.4131	11.4010	108	108	112	-47307.28
Li ₇ La ₃ Zr _{1.75} Nb _{0.25} O ₁₂	11.3875	11.3875	11.3811	108	108	112	-45891.34

3.3 Band structure and total state density analysis

The calculation structure of energy band and state density is shown in Figure 3-2(a~c) and Figure 3-3(a~f) to Figure 3-5(a~f). Related data of different energy bands near fermi level are recorded in Table 2-2, and fermi level is taken as zero point of energy.

According to the band diagram and Table 3-2, the band (a) of Li₇La₃Zr₂O₁₂ is mainly distributed between -47~25eV, and part of the band width is large, and there is overlap between adjacent orbits. The conduction bandwidth is 20.77eV, the upper valence bandwidth is 3.37eV, the lowest point of conduction band (3.96eV) and the highest point of valence band (0eV) are all at the same high symmetric point G, and Li₇La₃Zr₂O₁₂ crystal is a direct band gap. In addition, the band gap is 3.96eV, fermi level is at the top of upper valence band, which is similar to p-type semiconductor materials. The conductivity is determined by a small number of hole carriers, and the conductivity is low, which also indicates that Li⁺ is orderly arranged in tetetic phase structure.

After doping, the energy band moves to the direction of low energy, the number of bands increases and the bandwidth increases, especially the conduction band and valence band change obviously. The bottom of the conduction band passes through the fermi level, the energy required for electron transition decreases, and the free electrons in the conduction band increase. Compared with the P-type semiconductor, the conductivity improves and the conductivity increases. The widest conduction band and lowest band gap of Ta⁵⁺ doping system are 51.25eV and 2.74eV. The electrons are easier to transition and the conductivity is higher. Compared with (a), the conduction band and valence band of Nb⁵⁺ doping system increase, but the upper valence band increases slightly. The fermi level is located at the bottom of the conduction band, the band gap decreases slightly, and the change of conductivity is small. Similar to the results reported in literature [8,21], the conductivity of LLZO can be improved by doping.

The state density diagram corresponds to the band diagram, and different bands occupy different intervals in the state density diagram. According to the total state density diagram and energy band analysis, the state density diagram of doping at different positions is similar, but the peak strength and peak position of doping at different positions are different. The fermi energy levels are all located at the point where DOS is close to but not 0, and the crystal is mainly reflected in semiconductor properties, but has gold properties, which is the same as the result of energy band analysis. There are many local spikes in the valence band under the Fermi level. Zr doping leads to narrower and sharper corresponding energy band in the lower valence band.

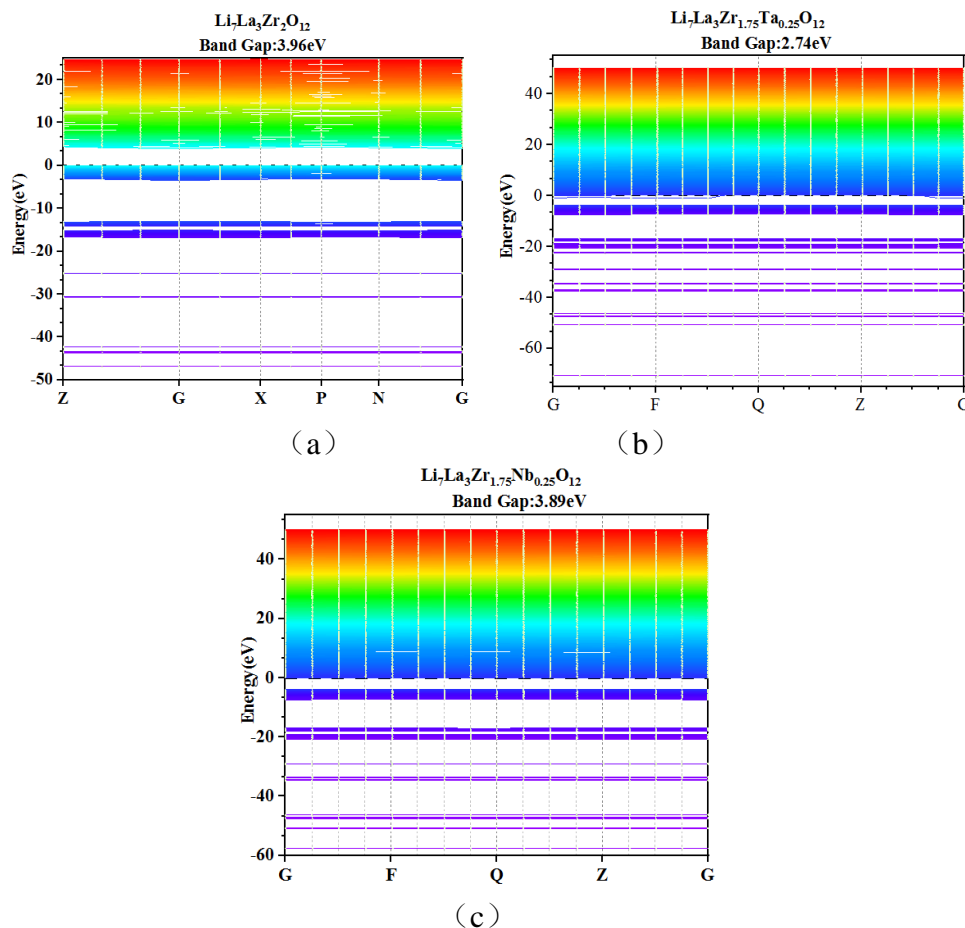


Figure 3-2 (a~c) Energy band diagram of different models

Table 3-2. Different energy band parameters

Structure	Range(eV)	Conduction Band(eV)	Valence Band(eV)	Band gap(eV)
Li ₇ La ₃ Zr ₂ O ₁₂	-46.89~24.73	3.96~24.73	-3.37~0	3.96
Li ₇ La ₃ Zr _{1.75} Ta _{0.25} O ₁₂	-70.73~50.15	-1.10~50.15	-7.42~-3.84	2.74
Li ₇ La ₃ Zr _{1.75} Nb _{0.25} O ₁₂	-57.46~50.09	0~50.09	-7.38~-3.89	3.89

The conduction band region of fermi level is widely distributed and uniform, and the peak value is lower. The electrons are relatively non-localized, and the atomic orbitals composed of the conduction band have strong expansibility.

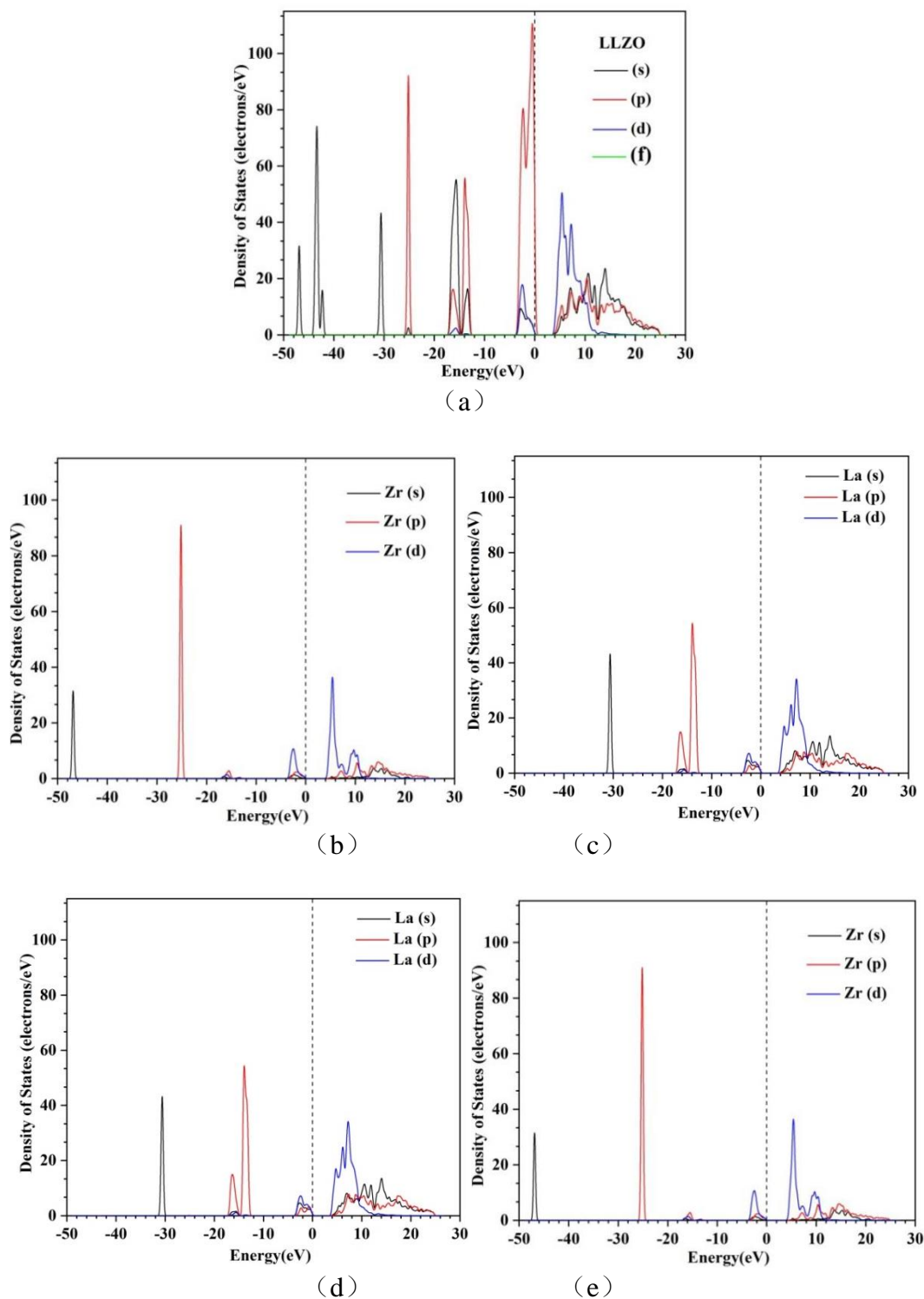


Figure 3-3 (a~e) LLZO and the partial density of states of each atom

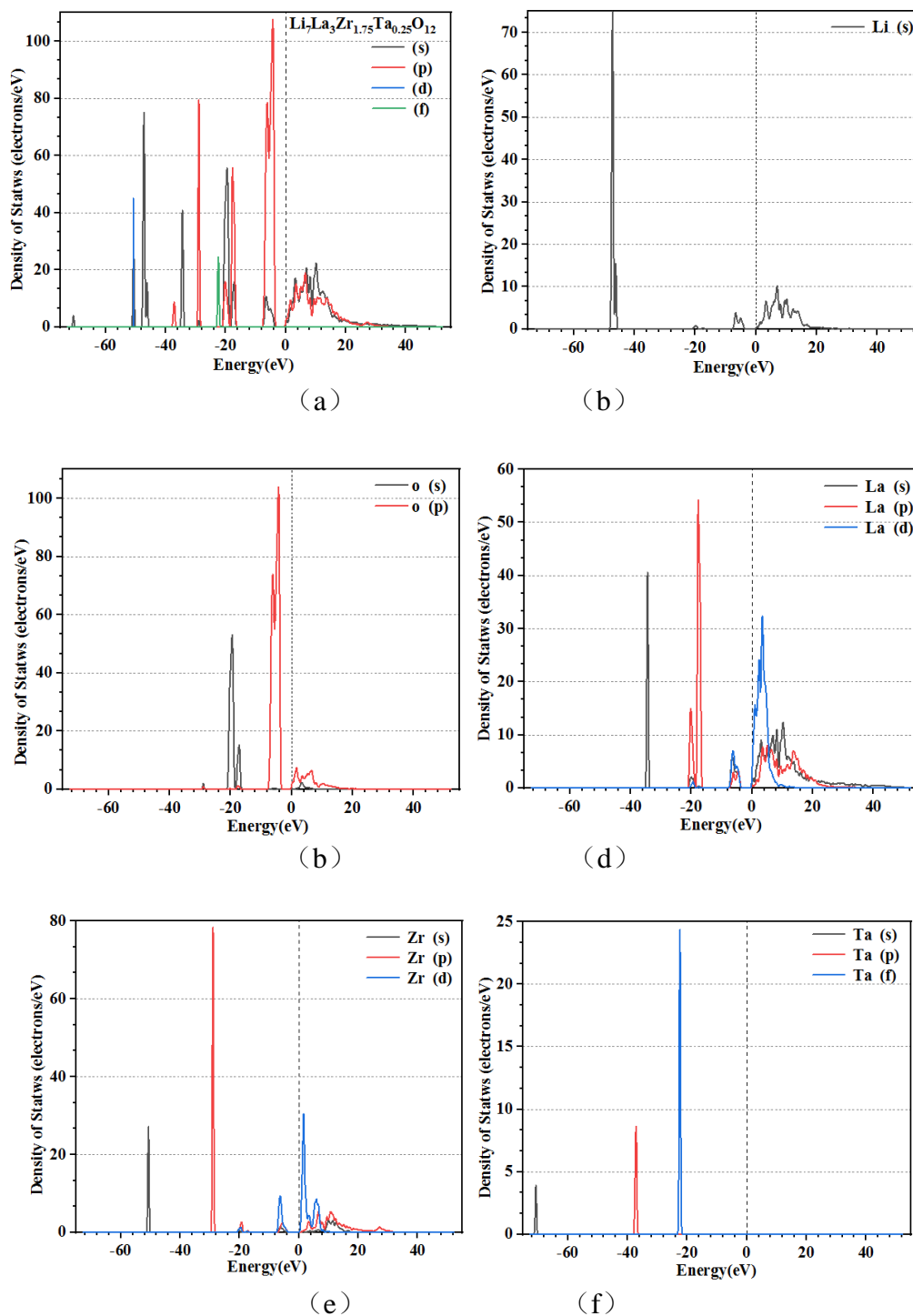


Figure 3-4 (a~f) $\text{Li}_7\text{La}_3\text{Zr}_{1.75}\text{Ta}_{0.25}\text{O}_{12}$ and the atomic density of states

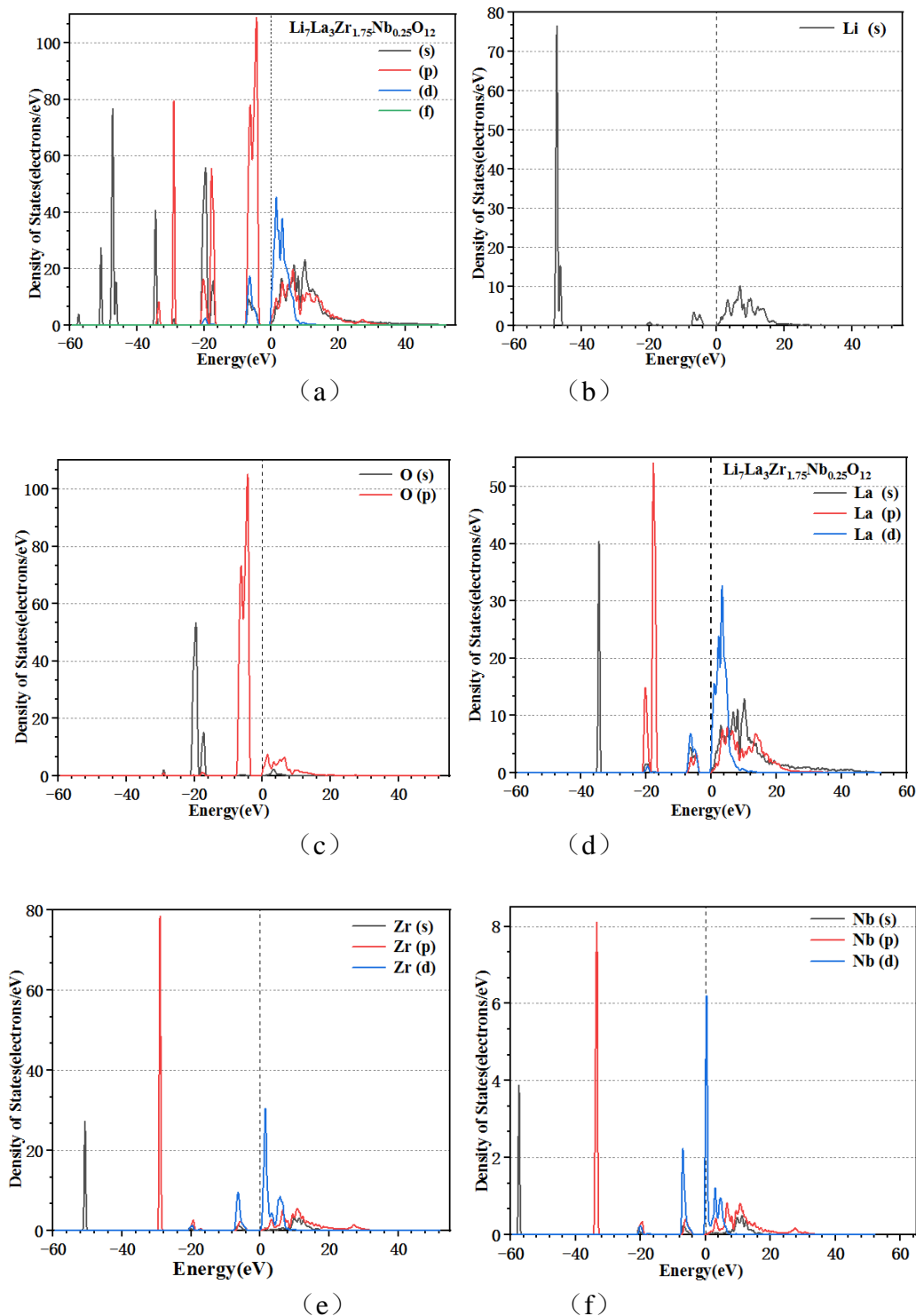


Figure 3-5 (a~f) $\text{Li}_7\text{La}_3\text{Zr}_{1.75}\text{Nb}_{0.25}\text{O}_{12}$ and the atomic density of states

In Addition, a new peak is added at -37.13eV 、 -22.46eV in Figure 3-4(a), and the energy band localization in the region of $-57.46\text{eV} \sim -3.89\text{eV}$ in Figure 3-5(a) is stronger, which is caused by the change of electronic structure due to the addition of electronic orbitals of Ta and Nb. Therefore, cationic

doping changes the size of the arrangement and migration channel of lithium ions in the crystal structure, which is conducive to improving structural stability and conductivity [23].

According to Fig.3-3(a~e) to Fig.3-5(a~f), the relationship between electron orbital and energy band and state density of different atoms is further analyzed. As can be seen from Fig.3-3, all energy bands in the $-48.56\sim 25.9\text{eV}$ region below the LLZO valence band are contributed by their respective atomic orbitals, and there is no overlap between the orbitals. In addition, the state density peaks of each band under the upper valence band are stronger and their widths are smaller, indicating strong localization. The upper valence band region near fermi level is the interaction of Li s-orbits, O p-orbits and p and d orbitals of La and Zr. There are two strong density peaks at -2.33eV and -0.464eV , which are mainly contributed by electrons from O 2p, La 5d and Zr 4d orbitals. The interatomic interaction is strong. However, the conduction band shows strong delocalization, and the electron orbitals of each atom contribute to form two obvious peak of state density, which is contributed by the 5d of La and the 4d of Zr. There is overlap between electron orbitals of different atoms, and Zr-O and La-O have strong interaction, which is consistent with LLZO crystal skeleton structure [9].

It can be seen from Fig.3-4 and Fig.3-5 that the density peaks of each atomic state are increased after Zr doping, which leads to the increase of the energy of the system. Near the fermi level, the conduction band is relatively wide, which is conducive to electronic transition and improves the conductivity. However, the delocalization between atomic orbitals is strong, covalent bond interaction is reduced, and the stability is relatively weakened. When Ta is doped, the conduction band is mainly contributed by Li, O, La and Zr orbitals, and the band generated at -37.13eV and -22.46eV in the lower valence zone is contributed by the p and d orbitals of Ta. In the upper valence zone, the peak of state density is sharp and localized, while in Nb doping, the peak of state density is most sharp, and all atomic orbitals contribute to the fermi level, and the interaction is strong, which is closer to the crystal structure of LLZO. According to the analysis of energy band and density of States, the electronic structure changes due to the electron orbital effect of doped elements. The doping of Ta and Nb will improve the conductivity of the material, and the doping effect of Ta is more significant.

3.4 Population analysis

The distribution of electrons in each atomic orbital is different, and the bonding status of each atom can be obtained by population analysis. The bond population analysis of LLZO system before and after doping is shown in Table 3-3, and the bond length is shown in Table 3-4.

As can be seen from Table 3-3 and 3-4, doping results in the increase of Li-O bond population, decrease of bond length and enhancement of bond covalency. Compared with the literature, the change of Li-O bond due to element doping tends to be the same [27]. Among them, the bond length of $\text{Li}_7\text{La}_3\text{Zr}_{1.75}\text{Ta}_{0.25}\text{O}_{12}$ is the smallest, indicating that the covalency of Li-O bond in this system is strong. With Ta doping, the La-O bond population decreases and the bond length increases, while the Zr-O bond population increases and the bond length decreases, indicating that the covalence of La-O bond is weakened while that of Zr-O bond is enhanced.

Table 3-3. bond population Average of crystals (e)

Bond	LLZO	$\text{Li}_7\text{La}_3\text{Zr}_{1.75}\text{Ta}_{0.25}\text{O}_{12}$	$\text{Li}_7\text{La}_3\text{Zr}_{1.75}\text{Nb}_{0.25}\text{O}_{12}$
Li-Li	0.123	0.092	0.104
Li-O	0.010	0.028	0.017
La-O	0.285	0.282	0.257
Zr-O	0.523	0.525	0.520
Ta-O	-	0.602	-
Nb-O	-	-	0.585

Table 3-4. Average bond length of crystals (Å)

Model	Li-Li	Li-O	La-O	Zr-O	Ta-O	Nb-O
LLZO	2.6471	2.2938	2.6010	2.1245	-	-
$\text{Li}_7\text{La}_3\text{Zr}_{1.75}\text{Ta}_{0.25}\text{O}_{12}$	2.5547	2.2610	2.6085	2.1257	2.1717	-
$\text{Li}_7\text{La}_3\text{Zr}_{1.75}\text{Nb}_{0.25}\text{O}_{12}$	2.6318	2.2865	2.6061	2.1228	-	2.2292

Because doping Ta results in the structural changes, the covalence of some bonds is enhanced or weakened, and a new Ta-O bond with bond length of 2.1717 Å is generated, which enhances the stability of the structure. With Nb doping, the population of La-O and La-O bonds decreases, the bond length increases, and the covalency of the bond weakens. Moreover, the bond length of the new Nb-O bond is 2.2292 Å, which is larger than that of Ta-O bond, so the stability of the system is low. In addition, the LLZO tetragonal structure has a higher Li^+ occupying rate and a lower conductivity due to the smaller coulombic repulsion between Li^+-Li^+ of the adjacent $[\text{LiO}_4]$ tetrahedron and $[\text{LiO}_6]$ octahedron. It is found through doping that the decrease of Li-Li bond length leads to the increase of Coulomb repulsion between Li^+-Li^+ , which is beneficial to the increase of Li vacancy concentration and conductivity. Compared with the experimental results in the literature, the results are consistent[28]. The minimum Li-Li bond length of $\text{Li}_7\text{La}_3\text{Zr}_{1.75}\text{Ta}_{0.25}\text{O}_{12}$ system is 2.5547 Å, combined with the analysis of energy band, its electrical conductivity is the highest. Therefore, doping different element has different effects on the conductivity of crystal structure, and it should also be related to the concentration of doped element, not the greater the better. At the same time, it is affected by the doping position, and the results are different.

4. CONCLUSION

(1) Through structural analysis, it is found that Nb doping leads to the increase of total energy, and the stability of the system decreases. After Ta doping LLZO system, the structure is more stable,

and the total energy is -47307.28eV.

(2) Band gap and band density analysis show that LLZO structure band gap is 3.96eV, fermi level is at the top of upper valence band, similar to p-type semiconductor material, conductivity is determined by a small number of hole carriers, low conductivity. Due to the effect of different Ta and Nb orbital electrons, the number of energy bands near the fermi level increases and the band gap decreases to 2.74eV (Ta) and 3.89eV (Nb). It is conducive to the transition of electrons or holes. The electron or hole transition energy is reduced, the conductivity is increased, Ta doping conductivity is relatively high.

(3) The population analysis shows that Li-O bond population increases, bond length decreases, and bond covalency is enhanced by doping. The bond length of $\text{Li}_7\text{La}_3\text{Zr}_{1.75}\text{Ta}_{0.25}\text{O}_{12}$ is the smallest, indicating that Li-O bond covalency is strong in the system. Doping Ta results in structural changes and the formation of a new Ta-O bond with bond length of 2.1717Å, which enhances the stability of the structure. With Nb doping, the bond length of La-O and La-O increases, and the covalency of the bond weakens. Moreover, the bond length of the newly generated Nb-O bond is 2.2292Å, which has lower stability compared with Ta doping system. On the other hand, the doping shows that the minimum Li-Li bond length of $\text{Li}_7\text{La}_3\text{Zr}_{1.75}\text{Ta}_{0.25}\text{O}_{12}$ system is 2.5547Å. The reduction of Li-Li bond length leads to the increase of coulomb repulsion between Li^+-Li^+ , which is conducive to the increase of Li vacancy concentration and the increase of electrical conductivity.

ACKNOWLEDGEMENT

This research was supported by the National Natural Science Foundation of China(No.51775042,52161033),Guangxi Natural Science Foundation (No. 2020GXNSFAA297082), the Fund Project of the GDAS Special Project of Science and Technology Development Guangdong Academy of Sciences Program (No.2020GDASYL-20200104030); the Innovation Project of Guangxi University of Science and Technology Graduate Education (YCSW2021324) Guangxi Innovation Driven Development Project (No.AA18242036-2).

References

1. J. M. Tarascon and M. Armand, *Nature*, 414 (2001) 6861.
2. M. Armand and J. M Tarascon, *Nature*, 451 (2008) 7179.
3. J. B. Goodenough and Y. Kim, *Chem. Mater*, 22 (2010) 3.
4. E. P. Roth and C. J. Orendorff, *Electro. Chem. Soc Inter.*, 21 (2012) 2.
5. X.S. Zhou, A.M. Cao , L.J. Wan, Y.G Guo, *Nano. Res.*, 5 (2012) 12.
6. Y. M. He, C. Y. Lu, S. Liu, W. J. Zheng and J. Y. Luo, *Adv. Energy. Mater.*, 9 (2019) 36.
7. R. Murugan, V. Thangadurai and W. Weppner, *Angew. Chem. Int. Edit.*, 46 (2017) 41.
8. V. Thangadurai, H. Kaack and W. J. F. Weppner. *J. Am. Ceram. Soc.*, 86 (2013) 3.
9. J. Awaka,N. Kijima, H. Hayakawa and J. Akimoto, *J. Solid. State. Chem.*, 182 (2019) 8.
10. R. Murugan, W. Weppner, P. S. Beurmann and V. Thangadurai, *Mater. Sci. Eng. B-Adv.*, 143 (2017) 1-3.
11. J. T. Han, J. L. Zhu, Y. T. Li, X. H. Yu, S. M. Wang, G. Wu, H. Xie, S. C. Vogel, F. Izumi, K. Momma, Y. Kawamura, Y. H. Huang, J. B. Goodenough and Y. S Zhao, *Chem. Commum.*, 48 (2012) 79.
12. R. Jalem, Yo. Yamamoto, H. Shiiba, M. Nakayama, H. Munakata,T. Kasuga and K. Kanamura,

- Chem. Mater.*, 25 (2013) 3.
13. N. Bernstein, M. D. Johannes and K. Hoang, *Phys. Rev. Lett.*, 109 (2012) 20 .
 14. S. Adams and P. Raor, *J. Mater. Chem.*, 22 (2012) 4.
 15. Y. T. Li, J. T. Han, C. A. Wang, H. Xie and J. B. Goodenough, *J. Mater. Chem.*, 22 (2012) 30.
 16. L. J. Miara, S. P. Ong, Y. F. Mo, W. D. Richards, Y. Park, J. M. Lee, H. S. Lee and G. Ceder. *Chem. Mater.*, 25 (2013) 15.
 17. S. Ramakumar, C. Deviannapoorani, L. Dhivya, L. S. Shankar and R. Murugan, *Prog. Mater. Sci.*, 88 (2017).325
 18. R. Jalem, M. Rushton, W. Manalastas, M. Nakayama, T. Kasuga, J. A. Kilner and R. W. Grimes, *Chem. Mater.*, 27 (2015) 8.
 19. L. Dhivya, N. Janani, B. Palanivel and R. Murugan, *Aip. Adv.*, 3 (2013) 8.
 20. K. Meier, T. Laino and A. Curioni. *J. Phys. Chem. C.*, 118 (2014) 13.
 21. L. J. Miara, W. D. Richards, Y. E. Wang and G. Ceder. *Chem. Mater.*, 27 (2015) 11.
 22. D. Rettenwander, Daniel, Geiger, A. Chailes, Amthauer, Georg, *Inorg. Chem.*, 52 (2013) 14.
 23. E. Y. Yi, W. M. Wang, J. Kieffer and R. M. Laine, *J. Power. Sources.*, 352 (2016).
 24. S. Ohta, T. Kobayashi and J. Seki, T Asaoka. *J. Power. Sources.*, 202 (2012) 1.
 25. T. Thompson, J. Wolfenstine, J. L. Allen, M. Johannes, A. Huq, I. N. Davida and J. Sakamoto, *J. Mater. Chem. A.*, 2 (2014) 33.
 26. W. H. Xia, B. Y. Xu, H. N. Duan, Y. P. Guo, H. M. Kang, H. Li and H. Z. Liu, *ACS. Appl. Mater. Inter.*, 8 (2016) 8.
 27. M Abdulai, K B Dermenci, S Turan. *Ceram. Int.*, 12(2021)0272.
 28. J Dai, Q Chen, T Glossmann, W Lai. *Comput. Mater. Sci.*, 162(2019) 333